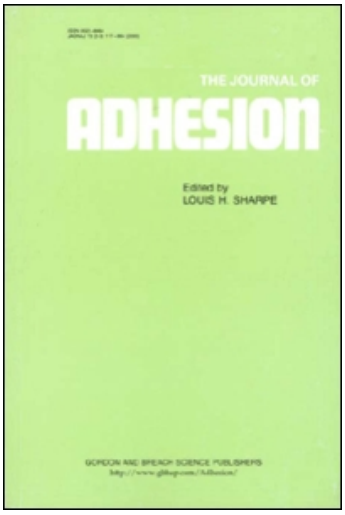

The Journal of Adhesion
Publication details, including instructions for authors and subscription information:
http://www.informaworld.com/smpp/title~content=t713453635

Failure Surface Analysis of Polyimide/Titanium Notched Coating Adhesion Specimens

Rachel Knudsen Giunta[a]; Ronald G. Kander[a]
[a] Materials Engineering Science, Virginia Polytechnic Institute and State University, Blacksburg, VA, USA

To cite this Article Giunta, Rachel Knudsen and Kander, Ronald G.(2001) 'Failure Surface Analysis of Polyimide/Titanium Notched Coating Adhesion Specimens', The Journal of Adhesion, 77: 3, 183 — 214
To link to this Article: DOI: 10.1080/00218460108030738
URL: http://dx.doi.org/10.1080/00218460108030738

The Journal of Adhesion, 77: 183–214, 2001

0021-8464/01 $12.00 + .00

Failure Surface Analysis of Polyimide/Titanium Notched Coating Adhesion Specimens

RACHEL KNUDSEN GIUNTA and RONALD G. KANDER

Materials Engineering Science, Virginia Polytechnic Institute and State University, Blacksburg, VA, USA

(Received 13 December 2000; in final form 5 July 2001)

Adhesively-bonded joints of LaRC™ PETI-5, a phenylethynyl-terminated polyimide, with chromic acid anodized titanium were fabricated and debonded interfacially. The adhesive-substrate failure surfaces were investigated using several surface analysis techniques. From Auger spectroscopy, field emission scanning electron microscopy, and atomic force microscopy studies, polymer appears to be penetrating the pores of the anodized substrate to a depth of approximately 100 nm. From X-ray photoelectron spectroscopy data, the polymer penetrating the pores appears to be in electrical contact with the titanium oxide, leading to differential charging. These analyses confirm that the polymer is becoming mechanically interlocked within the substrate surface.

Keywords: Polyimide; Interphase; PETI-5 Adhesive; Chromic Acid Anodization; Ti-6Al-4V; Pore Penetration

---

Presented at the 23rd Annual Meeting of The Adhesion Society, Inc., held at Myrtle Beach, South Carolina, USA, 20–23 February 2000.

The authors gratefully acknowledge the Center for Adhesive and Sealant Science at Virginia Tech and the Adhesive and Sealant Council Education Foundation for financial support. In addition, we would like to thank several members of the Composites and Polymers Branch, NASA Langley Research Center. We thank Terry St. Clair for providing materials and research facilities, and Mia Siochi and Jeffrey Hinkley for valuable discussions. Finally, we would like to thank Sandia National Laboratories for support of the preparation of this manuscript. Sandia is a multiprogram laboratory operated by Sandia Corporation, a Lockheed Martin Company, for the United States Department of Energy under Contract DE-AC04-94AL85000.

Present address of R. G. Kander: James Madison University, Integrated Science & Technology Department, ISAT/CS Building, MSC 4102, Room 321, Harrisonburg, VA 22807, USA.

Address correspondence to Rachel Knudsen Giunta, Sandia National Labs, MS0958, P. O. Box 5800, Albuquerque, NM 87185-0958, USA. E-mail: rgiunta@sandia.gov

INTRODUCTION

When bonded joints are subjected to harsh environmental conditions, failures tend to occur near the interface [1–5]. Therefore, the longterm durability of adhesive joints is critically dependent on the three-dimensional adhesive/substrate interphase. According to Venables [6], mechanical interlocking is critical for good initial bond strength and long-term durability of metal-polymer bonds. Mechanical interlocking, or *keying*, involves the flow of adhesive into interstices of the substrate surface. Subsequent solidification locks the adhesive into the "well". Mechanical interlocking is believed to contribute significantly to the adhesion of substrates that exhibit microroughness, such as metal surfaces treated with chromic acid anodization (CAA) or sodium hydroxide anodization (SHA).

Analysis of mechanical interlocking at the adhesive-substrate interphase is essential in the study of the durability of high-performance adhesives. A current area of adhesive durability research is the development of critical technologies for elevated temperature aerospace applications. High-performance polymeric adhesives are needed for bonding titanium in structural components of aircraft. These joints have been designed to withstand a temperature of 177°C for 60,000 hours while maintaining desirable mechanical properties [7].

LaRC™ PETI-5 [8–16], a phenylethynyl-terminated polyimide adhesive, was developed for potential use in high-temperature aircraft applications. The structure of the PETI-5 precursor, which undergoes chain extension and crosslinking of the end groups during cure, is illustrated in Figure 1. Prior to cure, the molecular weight of PETI-5 used in the current study is 5,000 g/mol. After an elevated temperature cure, the lightly-crosslinked, amorphous polyimide has a glass transition temperature of 260°C. The potential for use of PETI-5 in the aerospace industry has prompted numerous investigations of the durability of these adhesive joints with Ti-6Al -4V [12, 16, 17], an alloy of 90% titanium, 6% aluminum, and 4% vanadium.

The objective of the current study is to determine whether PETI-5 adhesive is penetrating the pores of the anodized titanium substrate during processing. Although previous studies of polyimides bonded to anodized substrates have stated the assumption that the adhesive is penetrating the pores of the substrate [18], direct evidence of

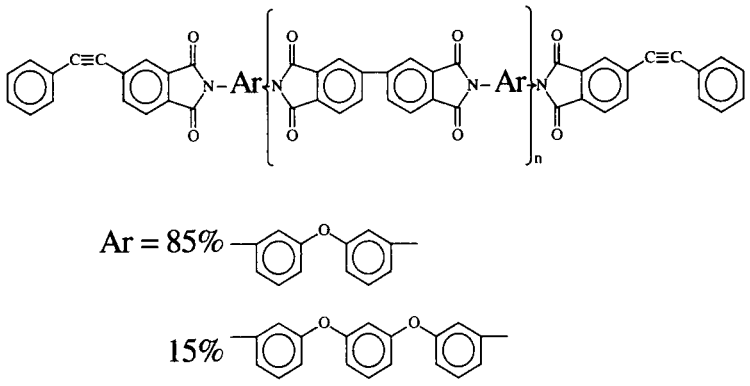

FIGURE 1 Structure of PETI-5 before cure. $\langle M_n \rangle = 5,000$ g/mol.

penetration has not been previously reported. Filbey and Wightman [19] found that an epoxy penetrated the pores of CAA Ti-6Al-4V, one of the limited number of pore penetration studies that have been reported [19, 20]. The difference in the chemistry and molecular structure of epoxies *versus* polyimides prevent one from assuming that their penetration behavior will be similar. In fact, the higher molecular weight and more rigid backbone structure of polyimides would render them less able to penetrate nanometer-scale pores than epoxies. Here, the penetration of PETI-5 into the pores of CAA Ti-6Al-4V is investigated using several surface analysis techniques.

EXPERIMENTAL

Materials

Adhesives

LaRC PETI-5, a phenylethynyl-terminated polyimide adhesive, was received from Imitec,™ Schenectady, NY, USA, as an amic acid solution at 35% solids (w/w) in N-methyl pyrrolidinone (NMP). The calculated molecular weight of uncured PETI-5 was 5,000 g/mol. Upon cure, PETI-5 is a thermoset with a T_g of 260°C.

PETI-5 adhesive tape was fabricated from the amic acid solution and used in the preparation of adhesive specimens. An E-glass scrim

cloth, 0.08 mm thick, with Al 100 finish, arranged in a 0°/90° plain weave, was stretched onto a frame and dried at 150°C for one hour prior to application of the adhesive. The cloth was impregnated with adhesive by applying PETI-5 as a poly(amic acid) solution in NMP using a natural bristle paintbrush. Each coat of PETI-5 solution was dried for one hour at 175°C. Several coats were applied to the glass cloth until the desired thickness of 0.30 mm was obtained. Further drying cycles up to 250°C were performed to reduce the volatile content of the tape to less than 2.5%.

Substrates

The substrates of all adhesive specimens were Ti-6Al-4V. Substrates, which measured 203 × 12.7 × 1.78 mm, were received from President Titanium Co., Hanson, MA, USA.

Following degreasing of the substrates, they were anodized in chromic acid at 5.0 V and 0.2 amps for 20 minutes. After drying in a 60°C oven, the PETI-5 coupons were primed using a 16% solids solution of PETI-5 amic acid in NMP. The primed coupons were dried at 225°C for 1 hour.

Adhesive Specimens

Notched coating adhesion (NCA) specimens [21, 22] of PETI-5 bonded to CAA-treated Ti-6Al-4V were analyzed for the current study. NCA specimens were selected to achieve interfacial failure, along with acceleration in aging that results from the specimen geometry [23].

Specimens were manufactured in an autoclave under vacuum using a bonding pressure of 690 kPa at 350°C for 30 minutes and 371°C for 30 minutes. Two plies of adhesive in scrim cloth were used, and bondlines were controlled to 0.25 mm.

Figure 2 illustrates an NCA specimen during debonding of the adhesive from the substrate. To debond the specimens along the adhesive/substrate interface, an initial cut was made between the adhesive and substrate of the NCA specimens by driving a razor blade into the interface. Specimens were then placed in a hand-held, three-point-bending fixture and bent so that the adhesive coating was in tension. The razor-induced debond propagated to form a sharp-tipped

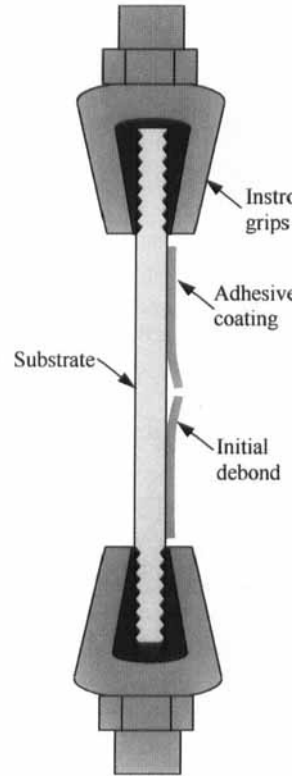

FIGURE 2 Schematic of a notched coating adhesion specimen during debonding.

debond between adhesive and substrate. Following initiation of the pre-crack, specimens were fitted with an extensometer and fully debonded by gripping the substrate in an Instron test frame and pulling the specimens in tension at a strain rate of 2.5 mm/min. This was accomplished on a 9 kN Instron test frame equipped with a System 4000 data acquisition system.

Aging Conditions

Some NCA specimens were aged for 30 days at 177°C in either air or nitrogen. Atmospheric pressure was maintained in all ovens. Unaged specimens were stored in a vacuum desiccator at room temperature until testing was performed.

Characterization

Optical Microscopy

Optical micrographs of failure surfaces were obtained using an Olympus BH-2 optical microscope. All failure surfaces, adhesive and metal failure sides, were analyzed.

Auger Electron Spectroscopy

Depth profiling was performed on a Perkin-Elmer model 610 scanning Auger system using a single-pass cylindrical mirror analyzer with electron excitation from a coaxial electron gun. The minimum electron beam diameter is less than 100 nm. The sputter rate was calibrated using a tantalum standard. AES was performed on the metal failure surface of three debonded specimens.

Field Emission Scanning Electron Microscopy (FE-SEM)

FE-SEM was performed on an LEO model 1550 Field Emission Scanning Electron Microscope at 0.25 to 2.0 kV. The adhesive and titanium failure surfaces of three debonded specimens were analyzed. Samples were not sputter-coated, and no charging was observed.

Atomic Force Microscopy

A Digital Instruments Dimension 3000 Atomic Force Microscope using the Nanoscope IIIa controller was used in tapping mode to obtain height and phase AFM images. The adhesive and metal failure surfaces of three specimens were analyzed.

X-ray Photoelectron Spectroscopy

To determine the atomic concentration of elements on the failure surfaces of NCA specimens, XPS was performed using a Perkin Elmer model 5400 spectrometer. A Mg Kα X-ray source operated at 14 kV (300 watts) of power was used to analyze a spot size of 1.0×3.0 mm on the specimen surfaces. Typical sampling depths are 5 to 10 nm, and the detection limits of the instrument reflect an atomic concentration

of approximately 0.2%. Both failure surfaces of six specimens were analyzed. Binding energies were standardized to the hydrocarbon portion of the spectrum at 285.0 eV.

RESULTS AND DISCUSSION

Adhesive Specimens

In the current study, the NCA specimen geometry was used as a convenient means of obtaining interfacial failure and acceleration of diffusion-controlled aging mechanisms. While strain energy release rates were not obtained for these specimens, similar NCA specimens prepared in our laboratory [23] showed a significant decrease in the critical strain energy release rate after aging for 30 days in air at 177°C. This drop in strength was accompanied by a decrease in the concentration of titanium oxide detected on the adhesive side of the failure surface, as determined by optical microscopy and XPS. The current specimens showed a similar decrease in the concentration of titanium oxide on the adhesive failure surface after aging in air for 30 days at 177°C. No change in the titanium oxide concentration was detected after aging in an inert nitrogen atmosphere for the same time and at the same temperature. The change in titanium oxide coverage on the failure surface indicates a change in the failure location as a result of aging in air at an elevated temperature. After aging, a higher percentage of the failure occurs in the adhesive, indicating weakening of the adhesive in the interphase region.

The concentration of titanium (in the form of TiO_2) on the adhesive failure surface of the current specimens, determined by XPS, is depicted in Figure 3. As can be seen in typical optical micrographs, Figure 4, the concentration of visible titanium oxide (light areas) on the adhesive failure surface (dark background) is noticeably decreased after aging in air. Again, aging in nitrogen has no apparent affect on the failure location. The effect of aging in air *versus* nitrogen is consistent with data reported by Parvatareddy [24] for a similar adhesive/substrate system. He found that the bond strength degrades more quickly during aging at elevated temperatures in air at atmospheric pressure, compared with aging in a reduced air pressure environment.

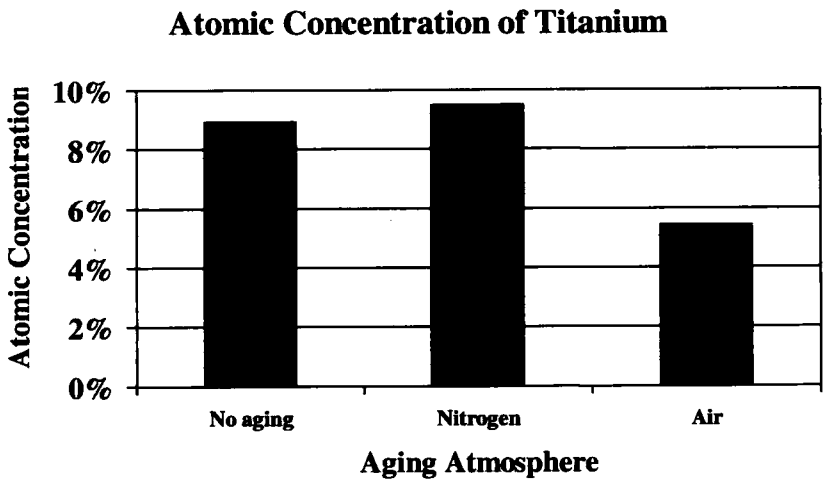

FIGURE 3 Atomic concentration of titanium on PETI-5 NCA adhesive failure surfaces, by XPS. Samples were aged for 30 days at 177°C in the indicated atmosphere.

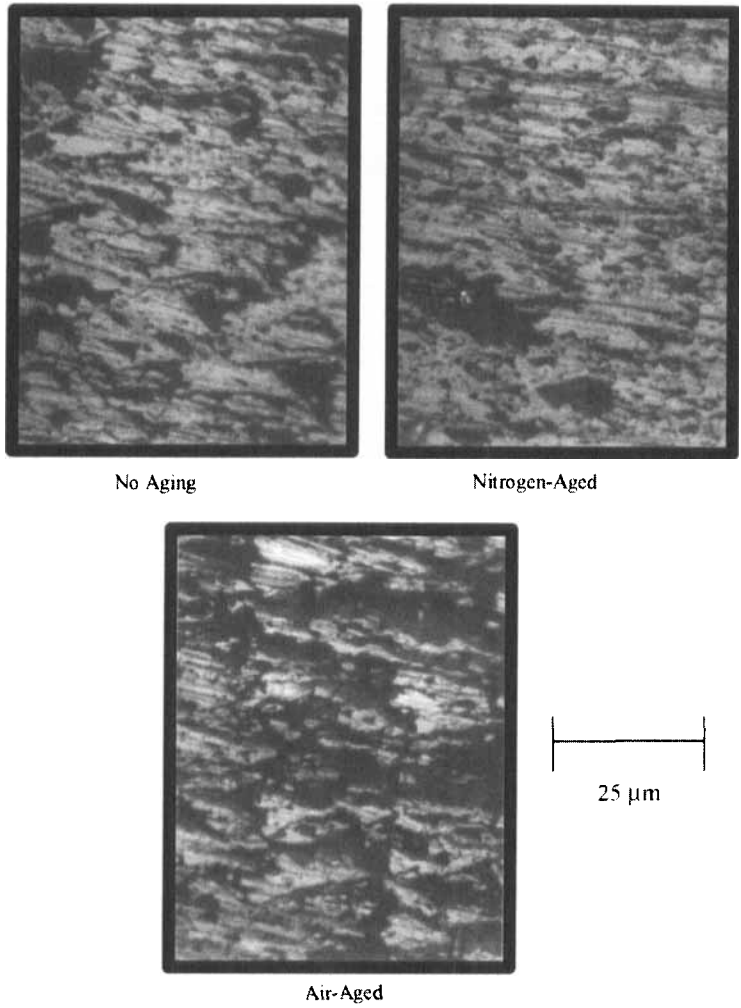

FIGURE 4 Optical micrographs of PETI-5 adhesive failure surfaces from NCA specimens. Specimens were aged for 30 days at 177°C in the indicated atmosphere.

Due to this change in failure location as a function of aging atmosphere, we believe that degradation of the adhesive at the interphase could be leading to decreased fracture toughness. This hypothesis would require that the adhesive and titanium oxide are strongly interpenetrated. Thus, this study investigates the penetration of polyimide adhesive into the pores of the CAA titanium oxide

surface. It should be noted that the images and data discussed are representative of all aging conditions. Despite the change in failure location and titanium oxide concentration as a function of aging time, no differences in microscopic features on the failure surfaces were observed.

Pore Penetration

Before looking for experimental evidence of pore penetration, we assessed if it is possible for PETI-5 polymer molecules to penetrate the porous oxide layer of CAA titanium. FE-SEM images of CAA Ti-6Al-4V are shown in Figure 5. The dark circular regions are pores in the CAA oxide layer, approximately 30 nm in diameter. When PETI-5 is applied to the anodized substrate surface, it is a primer in the form of a 16% solids amic acid solution in NMP. Using gel permeation chromatography, the radius of gyration of the PETI-5 amic acid solution was determined. The number-average radius of gyration was found to

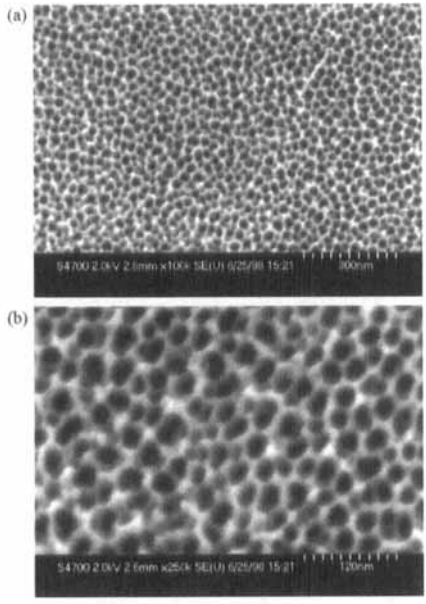

FIGURE 5 Field-emission scanning electron micrographs of a chromic acid anodized Ti-6Al-4V substrate surface.

be 3.6 nm, with weight-average and z-average radii of gyration of 4.8 and 5.7 nm, respectively. The diameter of the coiled polymer chain conformation, therefore, is less than the diameter of the substrate pores. Thus, it is reasonable to assume that PETI-5 amic acid can penetrate the pores of the CAA substrate.

Optical Microscopy

Titanium oxide was observed by optical microscopy on the adhesive failure surfaces of PETI-5 NCA specimens. In Figure 6, the adhesive and metal failure surfaces of a PETI-5 specimen are shown. These micrographs were taken in the same spot on corresponding adhesive and metal failure surfaces. On both failure surfaces, the light gray regions correspond to metal or metal oxide. Here, failure occurred in one of three locations: 1) through the metal oxide layer, 2) between the metal and metal oxide, or 3) through the metal itself. On the adhesive failure surface, Figure 6(a), dark features are observed which are mirror images of medium-gray features on the metal failure surface, Figure 6(b). The dark color on the adhesive failure surface, which was actually dark brown in color, is indicative of exposed PETI-5 adhesive. The medium-gray color on the metal failure surface was actually blue in color, and is consistent with the surface of anodized titanium. Although this appears to indicate interfacial failure between adhesive

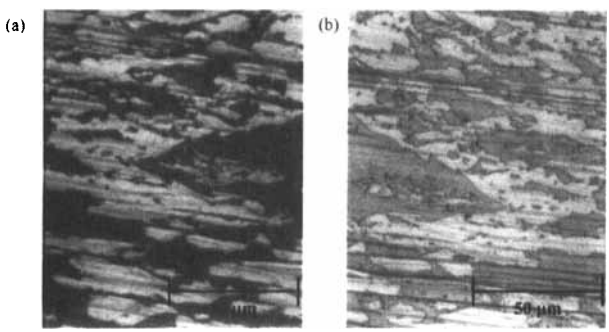

FIGURE 6 Optical micrographs of failure surfaces of a PETI-5 NCA specimen. (a) adhesive failure surface and (b) titanium failure surface. Micrographs were taken from failure surfaces in locations that were originally bonded to one another. Mirror images of features can be observed on the two failure surfaces.

and substrate, evidence of polyimide adhesive on the metal failure surface was consistently detected by XPS. Thus, there must be either a thin, optically-transparent coating of polyimide on the blue oxide layer or polyimide embedded within the pores of the oxide. To investigate this region further, Auger depth profiling, field-emission SEM, and atomic force microscopy were utilized.

Auger Electron Spectroscopy

Auger depth profiling of a PETI-5 metal failure surface, Figure 7, illustrates that carbon and titanium coexist in the top 75 to 100 nm of the failure surface. While this does imply the presence of polyimide at this depth, Auger data alone cannot be interpreted as confirmation of mechanically-interlocked polymer. Auger spectroscopy cannot distinguish between carbon as polyimide and carbon that may be present as a contaminant. However, if we tentatively assume that the presence of carbon represents polymer, we can construct a simple model of the interfacial region. Beyond the depth at which carbon is detected, oxygen (indicative of metal oxide) is present through an additional 50 nm. Deeper than this, only titanium and aluminum are detected. Thus, the polymer does not appear to penetrate the entire thickness of the titanium oxide layer. The validity of this interpretation of the Auger data can now be examined using additional surface analysis techniques. The model interphase is illustrated in Figure 8. The region in which adhesive and metal oxide are assumed to be present will be referred to as oxide A and the area in which there is only metal oxide is referenced as oxide B.

Scanning Electron Microscopy

Field-emission SEM was performed on the adhesive and metal failure surfaces of PETI-5 NCA specimens. Figure 9 is an FE-SEM of the metal failure surface. The features visible at this magnification are similar to those observed by optical microscopy. Dark areas correspond to the medium-gray regions of Figure 6(b), the anodized substrate surface, and light areas are exposed metal or metal oxide, present below the anodized region. Enlarging the center of Figure 9 by a factor of five, additional features become visible in Figure 10. The

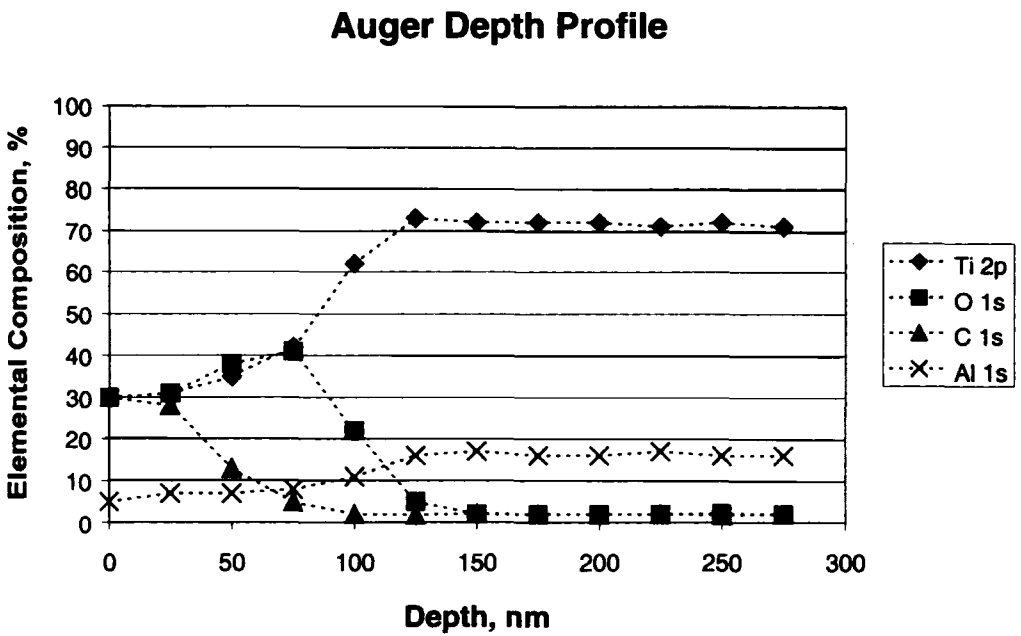

FIGURE 7 Auger electron spectroscopy depth profile of a PETI-5 metal failure surface from an NCA specimen.

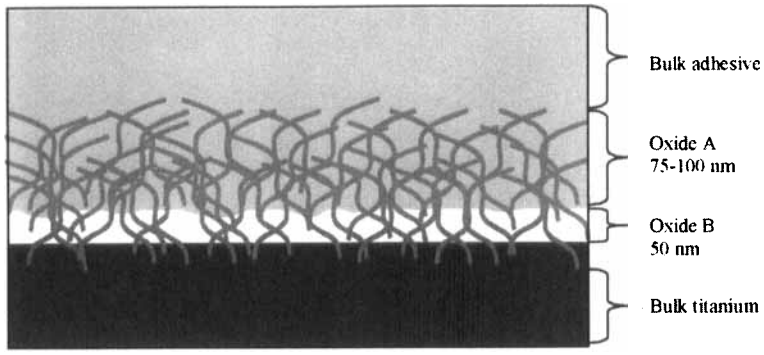

FIGURE 8 Schematic model of the PETI-5/CAA Ti-6Al-4V interphase based on Auger depth profiling data. Oxide A consists of the porous oxide layer embedded with adhesive. Oxide B is the porous oxide layer that contains no adhesive.

dark region on the left is the anodized substrate surface. The pores in the anodized oxide layer, which we believe to be infiltrated with polyimide adhesive, are clearly visible in this region. The failure here occurred between the bulk adhesive and the upper surface of oxide A. The porous structure of the lighter-colored region on the right side of the micrograph is apparent. Failure here occurred within the porous oxide layer. In the upper right corner of the micrograph, there is a circular region in which the porosity is not well defined. Here, it appears that the failure occurred at the interface of the porous and non-porous oxides.

In Figure 11, the edge of a porous oxide/polyimide region can be seen in another FE-SEM of a metal failure surface. This micrograph illustrates the sponge-like morphology through the thickness of the oxide layer. One can also see, from the scale of this micrograph, that the thickness of the oxide/polyimide layer is on the order of 100 nm, in agreement with the Auger depth profiling data and consistent with oxide A in our model interphase.

Additional features are observed in FE-SEMs of adhesive failure surfaces. Figure 12 is an FE-SEM of an adhesive failure surface. The dark region at the top of this micrograph corresponds to the dark brown adhesive observed by optical microscopy, Figure 6(a), while the lighter region on the bottom corresponds to the light gray metal oxide. Across the top of this micrograph, the ductility of the polymer is

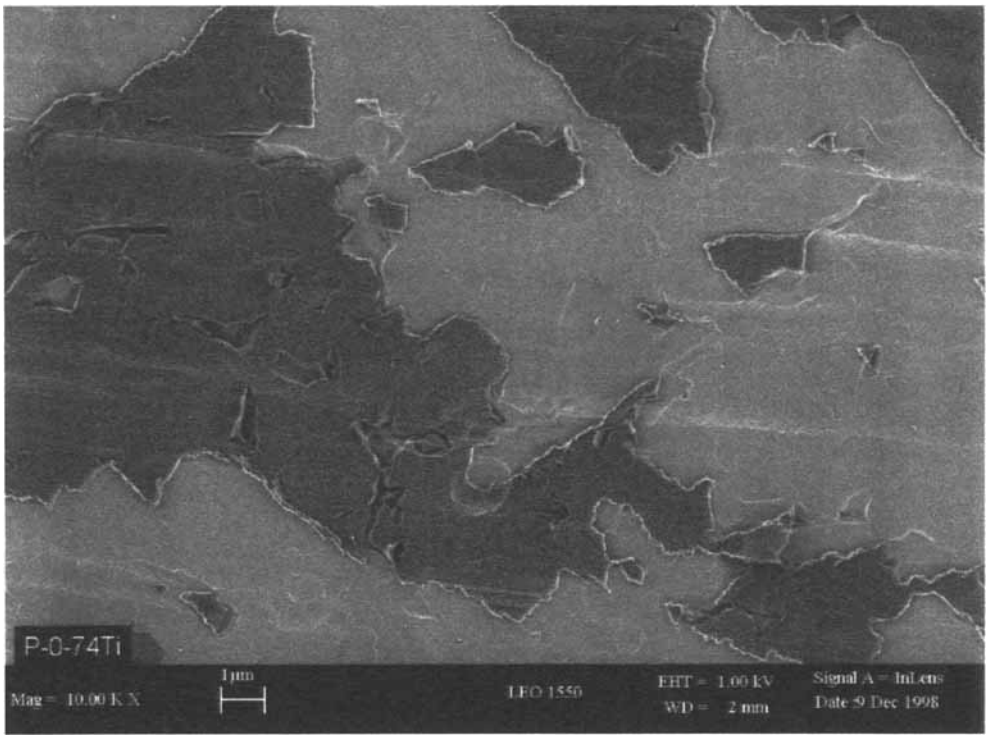

FIGURE 9 Field-emission SEM of the metal failure surface of a PETI-5 NCA specimen.

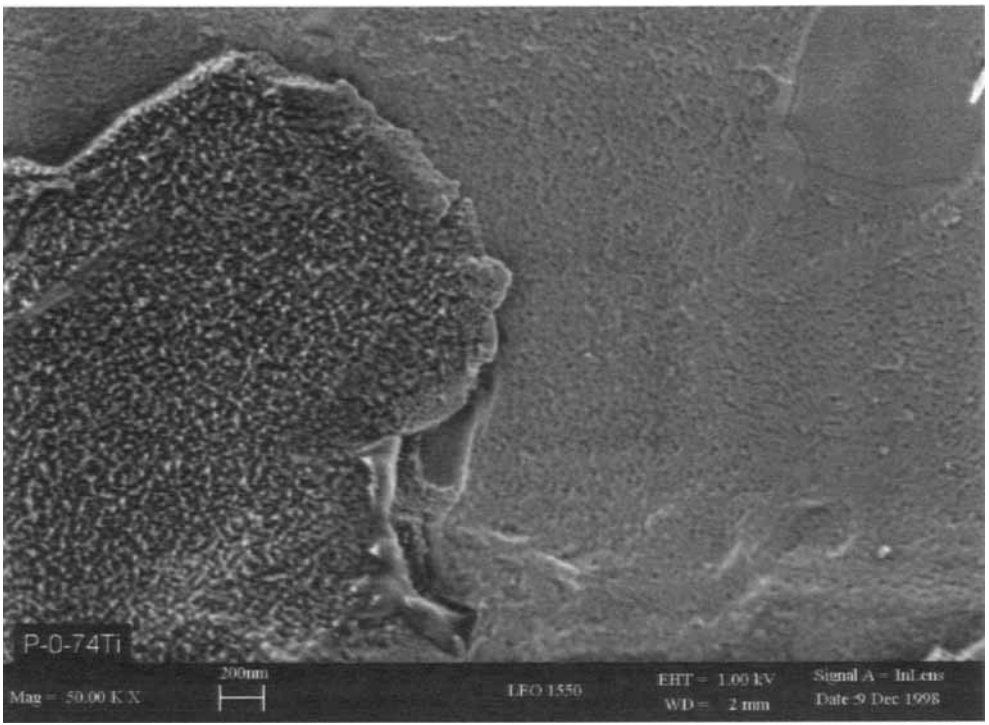

FIGURE 10 Field-emission SEM of the metal failure surface of a PETI-5 NCA specimen.

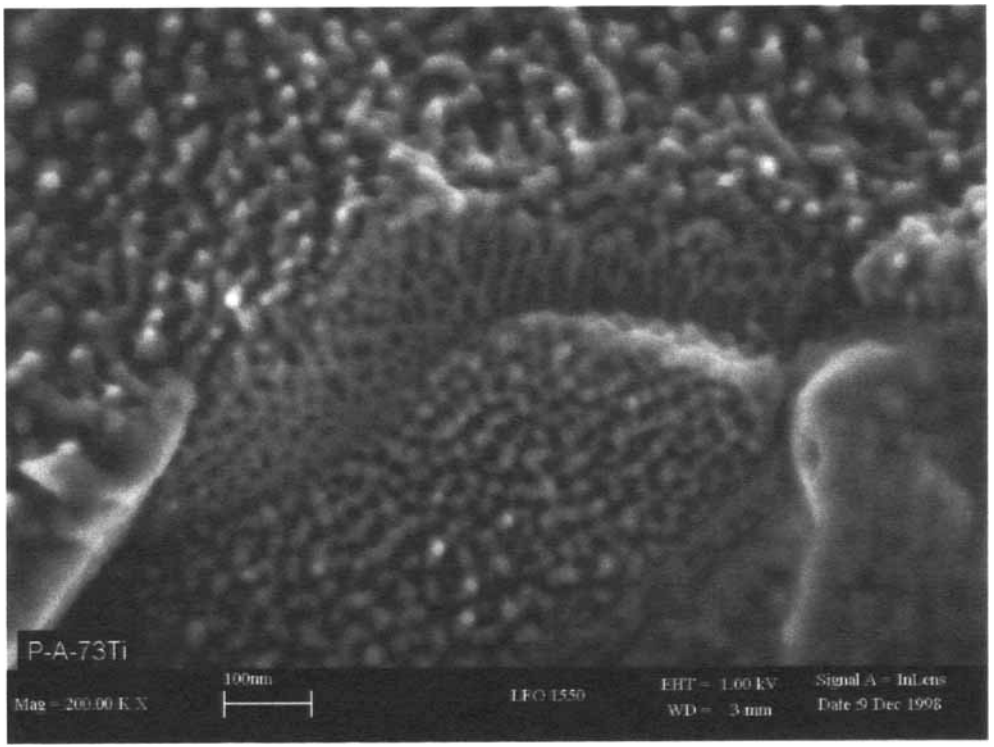

FIGURE 11 Field-emission SEM of the metal failure surface of a PETI-5 NCA specimen.

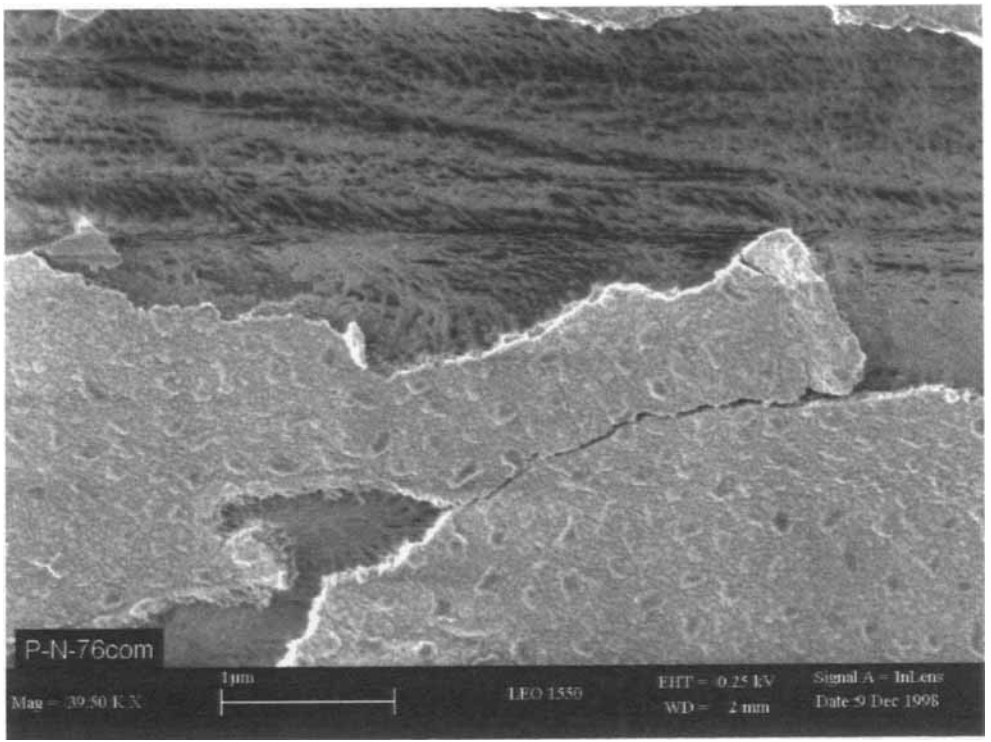

FIGURE 12 Field-emission SEM of the adhesive failure surface of a PETI-5 NCA specimen.

evident by the drawing and fibrillation that occurred as the failure propagated from the right to the left of this micrograph. In the lower half of the micrograph, the titanium failure region is observed. On this metal oxide surface, round features of two sizes can be seen. These features are enlarged in Figure 13. The smaller features are round, uniform, and less than 50 nm in diameter. The size, shape, and spatial distribution of the smaller features are consistent with the pores on the anodized titanium surface in Figure 5. Thus, we believe these are either the pores themselves or polymer that has been pulled from the pores on the metal failure surface. The larger features are irregular in shape and range from 150 to 400 nm across. We believe that they represent clusters of pores. These features were analyzed further using AFM.

Atomic Force Microscopy

Atomic force microscopy was used to determine if the round features observed in FE-SEM micrographs were raised (polymer) or indented (pores). The larger features are believed to be the result of the failure propagating through the walls of several pores in close proximity. AFM images of the metal failure surface and the adhesive failure surface are shown in Figure 14 and Figure 15, respectively. Note that the scales in the two micrographs are different. The 30 nm pores cannot be resolved by AFM; however, the larger features (approximately 200 nm) observed in Figure 13 appear in a periodic fashion in the AFM images.

In the AFM height images, on the left in each figure, lighter shades correspond to higher features. In Figure 14, the metal failure surface, the dark background is exposed oxide. The diagonal strip of lighter color is the anodized oxide layer (*i.e.*, the medium-gray regions of Figure 6(b)). The small features on the background oxide surface are darker than the background and, therefore, indented. On the adhesive failure surface, Figure 15, features of approximately the same size are raised, illustrated by the fact that they are lighter in color than the background. The matching raised features on the adhesive failure surface and indented features on the metal failure surface support the assertion that polyimide adhesive is embedded in the pores of the CAA oxide layer. From the model proposed in Figure 8, the failure within the oxide layer appears to be occurring at the interface of oxide A and oxide B. The raised features on the adhesive failure surface would then

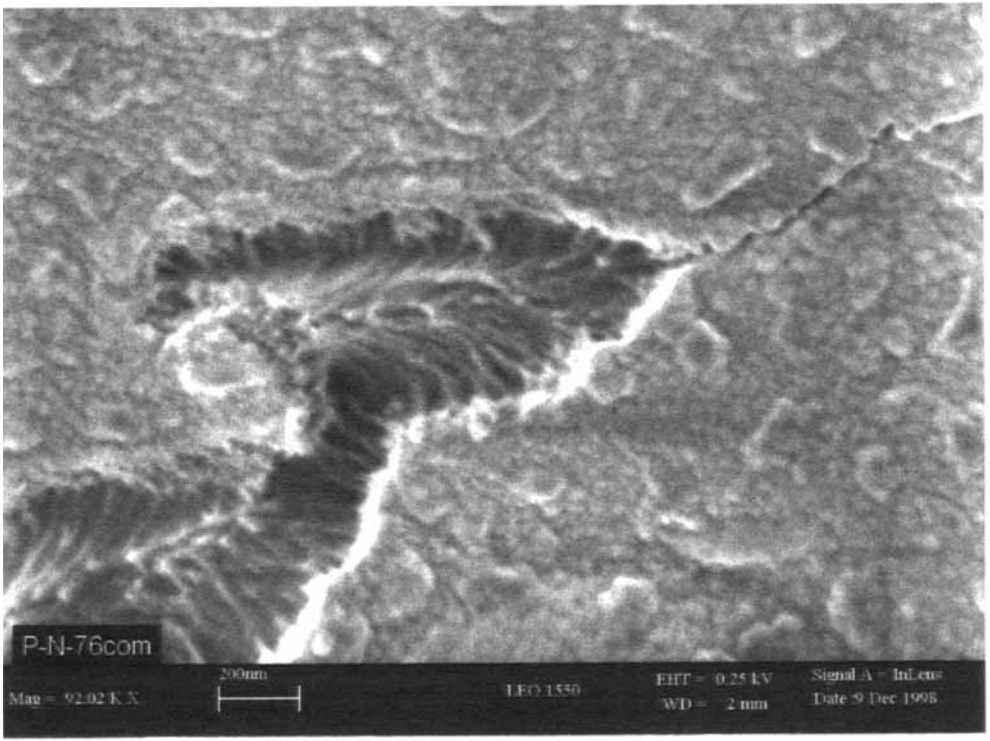

FIGURE 13 Field-emission SEM of the adhesive failure surface of a PETI-5 NCA specimen.

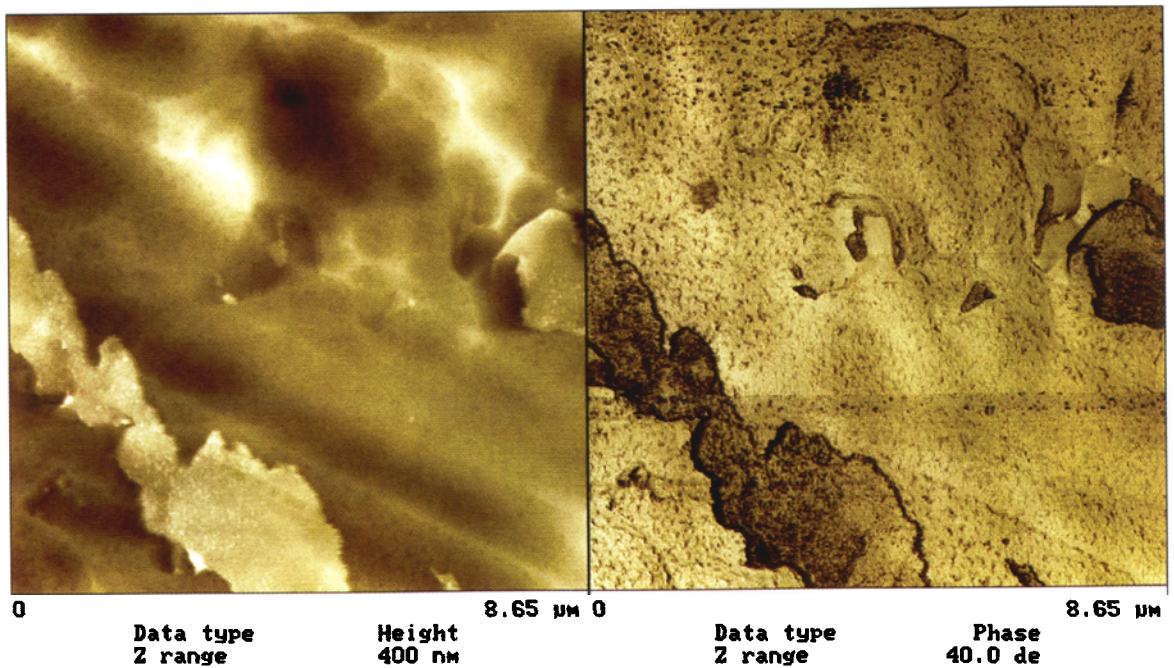

FIGURE 14 Height (left) and phase (right) atomic force microscopy images of the metal failure surface of a PETI-5 NCA specimen.

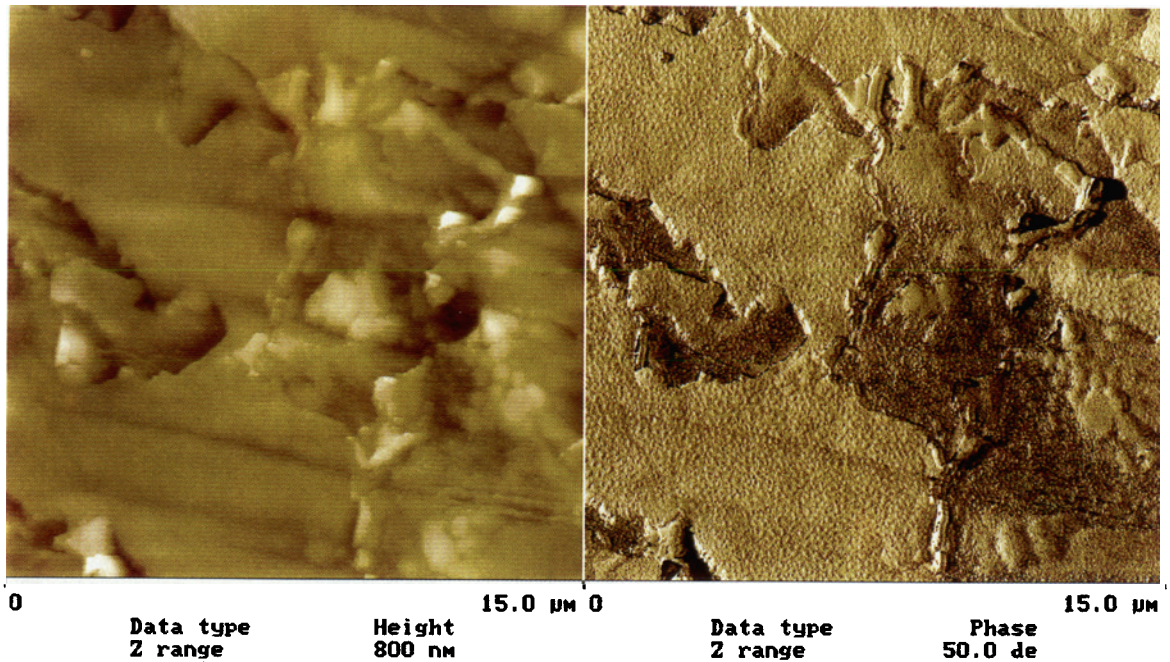

FIGURE 15 Height (left) and phase (right) atomic force microscopy images of the adhesive failure surface of a PETI-5 NCA specimen.

be attributed to polymer embedded in the oxide, and the indented features in the metal oxide layer would be holes left in the oxide layer, having been pulled out by the polymer. Had the failure occurred through porous oxide that did not contain adhesive, these features would have appeared indented on both failure surfaces.

Additional information is obtained from the AFM phase images. Darker regions of the phase image indicate a higher phase lag that, in general, means dark areas are softer than light areas. The diagonal strip on the metal failure surface, Figure 14, is both higher and softer than the surrounding area. If there were no polymer embedded in the porous oxide, it would not be softer than the surrounding metal oxide. This again confirms that the substrate pores contain polyimide. All surface analysis data appear to validate the model in Figure 8. Thus, it is concluded that PETI-5 is penetrating the pores of the CAA substrate and becoming mechanically interlocked.

X-ray Photoelectron Spectroscopy

XPS analysis of adhesive failure surfaces of PETI-5 NCA specimens supports the conclusion that the polyper is embedded in the pores of the titanium substrate surface. Table I lists the XPS photopeak binding energies for N 1s, O 1s, Ti $2p_{3/2}$, Al $2p_{3/2}$, and F 1s referenced to the C

TABLE I Binding energies of XPS photopeaks on PETI-5 failure surfaces, referenced to the C 1s peak at 285.0 eV, with 95% confidence intervals

	Binding energy, eV			
XPS Photopeak	*Adhesive failure surface*	*Metal failure surface*	*CAA Ti-6Al-4V reference*	*Literature value* [25]
N 1s	400.5 ± 0.1	400.5 ± 0.1	400.3 ± 0.1[a]	400.9[b]
O 1s	532.4 ± 0.2	530.2 ± 0.1	530.3 ± 0.1[c]	530.0[d]
		531.7 ± 0.1		531.1[e]
Ti $2p_{3/2}$	461.0 ± 0.2	458.8 ± 0.1	458.9 ± 0.1	458.7[d]
Al $2p_{3/2}$	77.0 ± 0.2	74.3 ± 0.1	74.6 ± 0.1	74.3[e]
F 1s	687.8 ± 0.2	685.3 ± 0.2	685.0 ± 0.1	685.1[f]

[a] No polyimide was present on the reference sample. The N 1s, present at $\sim 1\%$, is believed to be a contaminant.
[b] as Kapton™ polyimide.
[c] The Al_2O_3 component appears as an unresolved shoulder.
[d] as TiO_2.
[e] as Al_2O_3.
[f] as CaF_2.

1s photopeak at 285.0 eV. (Note: Aluminum is a component of the Ti-6Al-4V alloy, and fluoride is present from a step in the anodization procedure.) Peaks resulting from elements on the substrate surface, Ti $2p_{3/2}$ Al $2p_{3/2}$, and F 1s, are shifted to a higher binding energy on the adhesive failure surface. These elements are present as TiO_2, Al_2O_3, and fluoride ion. On the metal failure side, titanium, aluminum, and fluorine are present at the expected chemical shifts, corresponding to the position of the anodized titanium reference and literature values [25] listed in Table I. On the adhesive failure surface, however, the Ti $2p_{3/2}$. Al $2p_{3/2}$, and F 1s peaks are shifted to approximately 2.5 eV higher binding energy than expected. In addition, the low energy (inorganic) portion of the O 1s spectrum has increased by 2.2 eV to overlap the organic portion of the spectrum. We believe that the shift in binding energy on the adhesive failure surface is the result of differential charging. This is analogous to the observation by Pertsin *et al.* [26] of differential charging on a sample consisting of platinum islands on a polymer film.

XPS analysis is prone to differential charging in situations where the analyzed surfaces exhibit inhomogeneous conductivity and electron affinity [27–30]. While performing XPS, the outgoing photoelectron leaves a positive charge on the sample surface. In an insulator, the spectrometer cannot conduct electrons to the sample surface to compensate for this charge. Consequently, a positive charge is built up on the specimen under analysis. While uniform charging of a non-conductor shifts the whole spectrum, generally to higher binding energies, differential charging causes different components of a sample to shift by different amounts. Thus, the typical means of correcting for uniform charging, such as the use of adventitious carbon as a binding energy reference, supply erroneous binding energies for a portion of the sample components [31].

In the current example, the charging of the adhesive and metal oxide is non-uniform. In referencing the entire spectrum to the C 1s photopeak at 285.0 eV, we have corrected for the charging of the organic adhesive but have displaced the positions of the substrate elements by 2.5 eV. Ti $2p_{3/2}$ XPS photopeaks from the metal and adhesive failure surfaces of PETI-5 NCA specimens are given in Figure 16, illustrating the shift caused by differential charging on the adhesive failure surface.

An additional effect, also believed to be caused by differential charging, is observed in the XPS data. The C 1s XPS photopeaks of

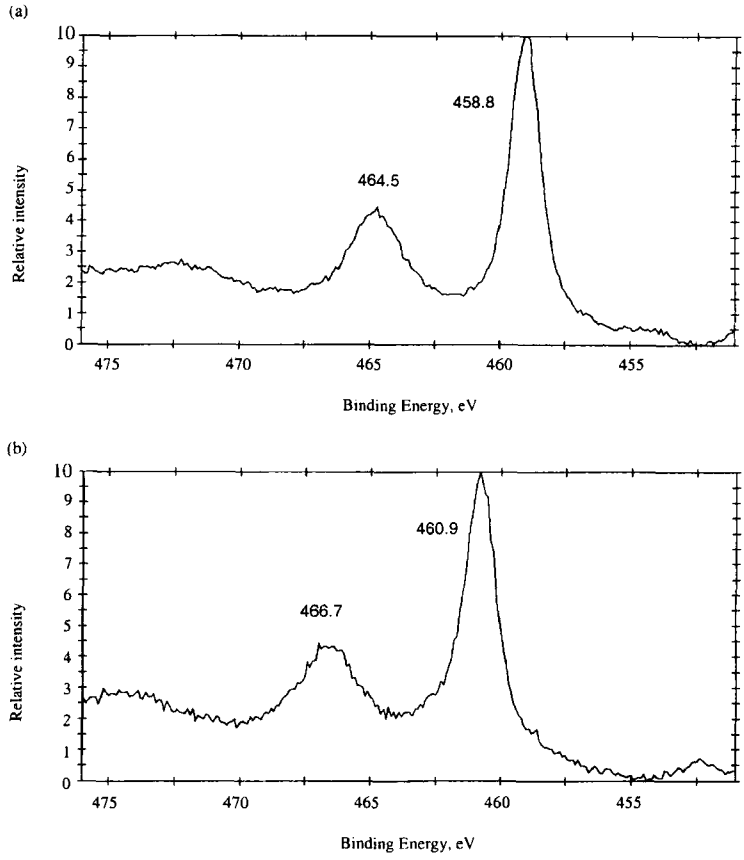

FIGURE 16 Ti $2p_{3/2}$ XPS spectra from (a) PETI-5 metal failure surface and (b) PETI-5 adhesive failure surface. Note: Each spectrum is on a normalized x-axis scale: as shown, peak heights and areas cannot be compared between the two spectra.

the metal and adhesive failure surfaces are shown in Figure 17. While both C 1s photopeaks have been resolved with four sub-peaks in approximately the same position, the peak at 287.0 eV on the adhesive failure surface is considerably larger than the corresponding peak on the metal failure surface. The peak position on the adhesive failure surface is also shifted to a slightly higher binding energy than that observed on the metal failure surface, 286.4 eV. Average binding energies for the four C 1s sub-peaks on the adhesive and metal

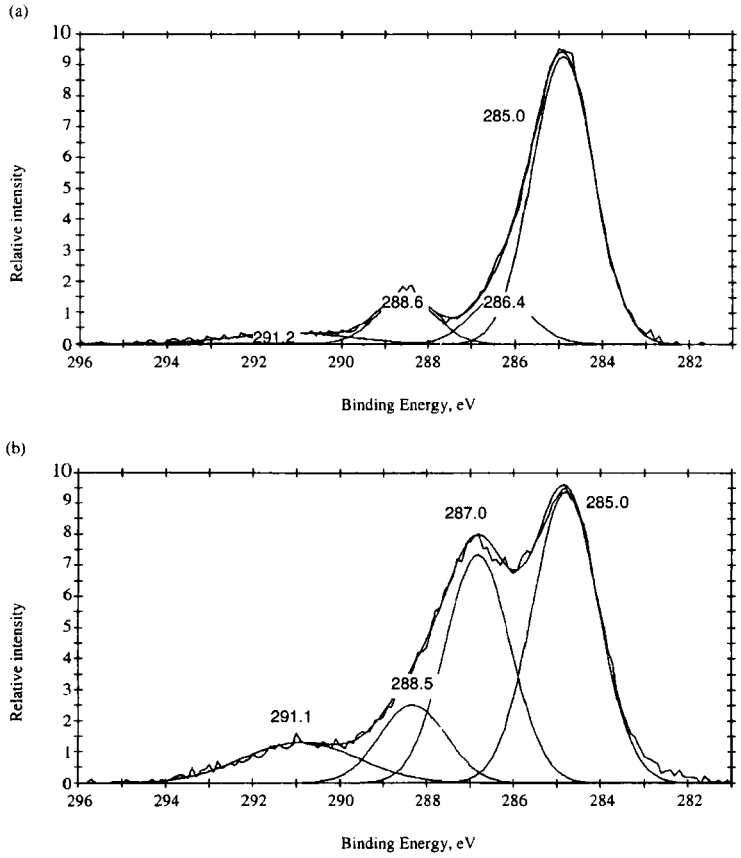

FIGURE 17 C 1s XPS spectra from (a) PETI-5 metal failure surface and (b) PETI-5 adhesive failure surface. Note: Each spectrum is on a normalized x-axis scale: as shown, peak heights and areas cannot be compared between the two spectra.

failure surfaces are listed in Table II. The peak at 286.4 eV is assigned to carbon single-bonded to oxygen. An additional feature obscures the C–O peak on the adhesive failure surface. The peak at 286.9 eV is believed to arise from the C–H component of the PETI-5 adhesive that is embedded in the porous TiO_2 substrate surface, the adhesive portion of oxide A. If the polymer is in electrical contact with the titanium, they are expected to undergo differential charging in unison [26]. In Figure 18, the percentage of the C 1s photopeak

TABLE II Binding energies of C 1s XPS sub-peaks on PETI-5 failure surfaces, referenced to the C 1s C–H sub-peak at 285.0 eV, with 95% confidence intervals

	Binding energy, eV	
XPS Photopeak	*Adhesive failure surface*	*Metal failure surface*
Peak 1	285.0	285.0
Peak 2	286.9 ± 0.1	286.4 ± 0.1
Peak 3	288.5 ± 0.1	288.6 ± 0.1
Peak 4	291.1 ± 0.1	291.1 ± 0.1

that has shifted to 286.9 eV is plotted as a function of titanium concentration. The portion of the C 1s peak that is shifted to higher binding energy is proportional to the amount of titanium detected on the surface. Note that the shifted component has been normalized by the total carbon concentration. The R^2 value of 0.88 indicates a strong linear fit, and the p-value of 0.017 indicates a 98.3% probability that the trend is significant. The relationship between the titanium detected on the surface and the amount of shifted carbon illustrates that the shifted carbon originates from polymer embedded in the pores of the oxide. To further illustrate this point, the C 1s

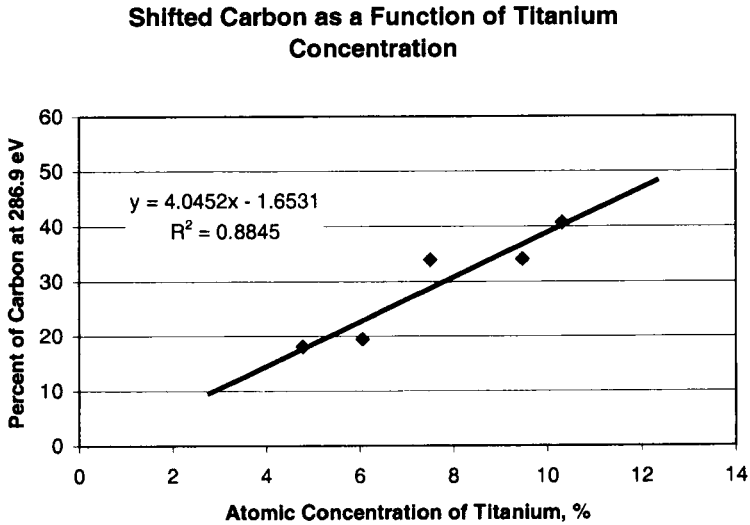

FIGURE 18 From XPS analysis of the PETI-5 adhesive failure surface, percent of the C 1s photopeak that is shifted to 286.9 eV as a function of titanium coverage.

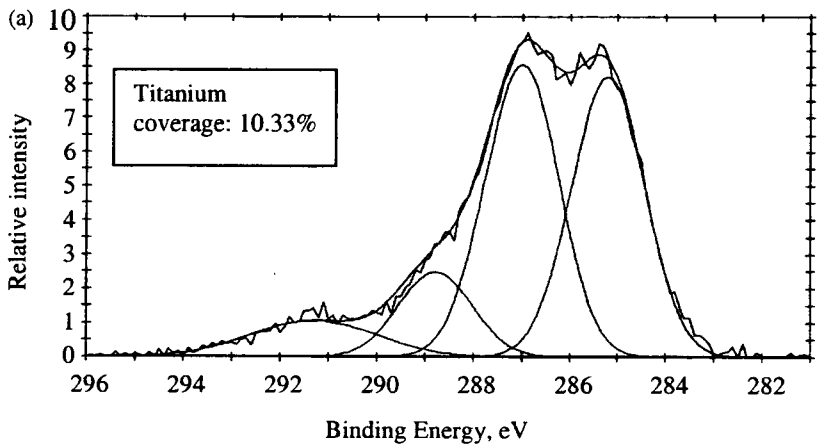

FIGURE 19 C 1s XPS spectra from PETI-5 adhesive failure surface with varying titanium coverage. Note: Each spectrum is on a normalized x-axis scale: as shown, peak heights and areas cannot be compared among the three spectra.

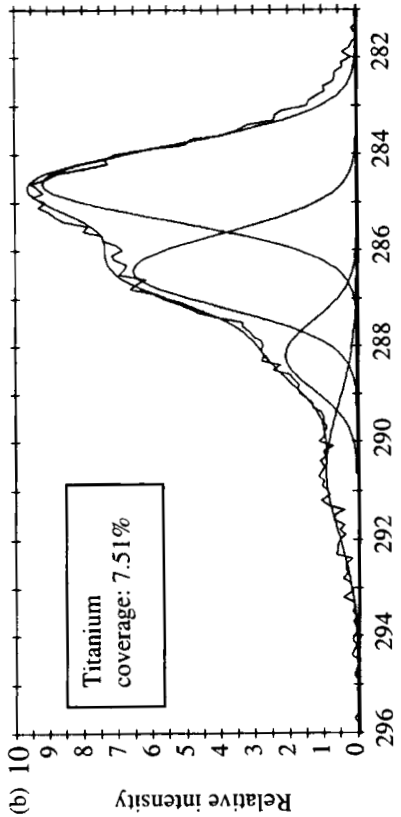

FIGURE 19 (Continued).

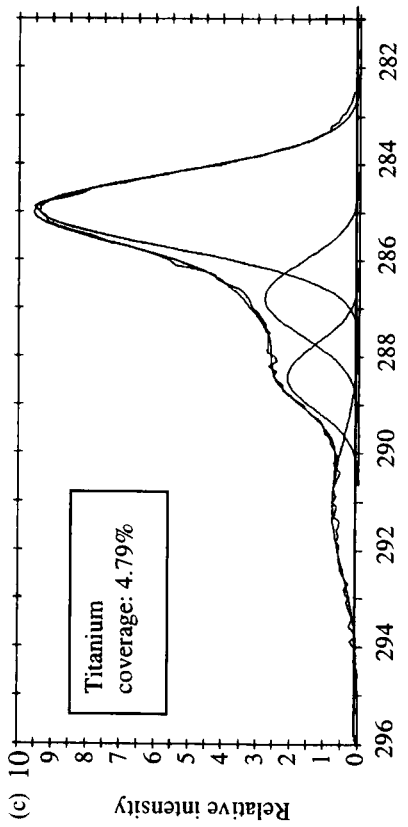

FIGURE 19 (Continued).

photopeaks of three adhesive failure surfaces are presented in Figure 19 along with the titanium coverage detected by XPS in the same sample. This clearly illustrates the decrease in the shifted portion of the C–H photopeak with decreasing titanium coverage. The charging component of the C-H peak, therefore, is attributed to polymer that is embedded in the porous oxide, or oxide A from the model discussed previously.

CONCLUSIONS

The interface of PETI-5 with CAA Ti-6Al-4V was investigated using several surface analysis techniques. From Auger spectroscopy, field emission SEM, and AFM studies, polymer is believed to be penetrating the pores of the anodized substrate to a depth of approximately 100 nm. From XPS data, this polymer appears to be in electrical contact with the titanium oxide, leading to differential charging. These analyses confirm that the polymer is becoming mechanically interlocked within the substrate surface.

References

[1] Fay, P. A. and Madison, A., *International J. Adhesion, Adhesives* **10**, 179 (1990).
[2] Watts, J. F., Castle, J. E. and Hall, T. J., *J. Mater. Sci. Lett.* **7**, 176 (1988).
[3] Kinloch, A. J., *J. Adhesion* **10**, 193 (1979).
[4] Kinloch, A. J., Shaw, S. J. and Hunston, D. L., *Polymer* **24**, 1355 (1983).
[5] Raveh, A., Marouani, D., Yolgar, R., Klemberg-Saphieha, J. E. and Bettelheim, A., *J. Adhesion* **36**, 109 (1991).
[6] Venables, J. D., *J. Mat. Sci.* **19**, 2431 (1984).
[7] Hergenrother, P. M. and Rogalski, M. E., *Polym. Prepr.* **33**(1), 354 (1992).
[8] Smith, J. G. and Hergenrother, P. M., *Polym. Prepr.* **35**(1), 353 (1994).
[9] Hergenrother, P. M. and Smith, J. G., *Polymer* **35**, 4857 (1994).
[10] Hergenrother, P. M., Bryant, R. G., Jensen, B. J. and Havens, S. J., *J. Polym. Sci. Poly. Chem. Ed.* **32**, 3061 (1994).
[11] Hinkley, J. A. and Jensen, B. J., *High Perform. Polym.* **7**(1), 1 (1995).
[12] Jensen, B. J., Bryant, R. G., Smith, J. G. and Hergenrother, P. M., *J. Adhesion* **54**(1), 57 (1995).
[13] Hou, T. H., Jensen, B. J., and Hergenrother, P. M., *J. Composite Materials* **30**(1), 109 (1996).
[14] Hinkley, J. A. and Jensen, B. J., *High Perform. Polym.* **8**, 599 (1996).
[15] Cano, R. J., Rommel, M., Hinkley, J. A. and Estes, E. D., *Proc. 41st International SAMPE Symposium*, Schmitt, G., Bauer, J., Magurany, C. J., Hurley, C. and Kliger, H. Eds., p. 1047 (1996).
[16] Cano, R. J. and Jensen, B. J., *J. Adhesion* **60**, 113 (1997).

[17] Parvatareddy, H., Dillard, J. G., McGrath, J. E. and Dillard, D. A., *J. Adhesion Sci. Technol.* **12**, 615 (1998).
[18] Ratta, V., Stanick, E. J., Ayambem, A., Parvatareddy, H., McGrath, J. E. and Wilkes, G. L., *Polymer* **40**, 1889 (1999).
[19] Filbey, J. A., Wightman, J. P., *J. Adhesion* **28**, 1 (1989).
[20] Packham, D. E., In: *Adhesion Aspects of Polymeric Coatings*, Mittal, K. L., Ed. (Plenum, New York, 1983).
[21] Chang, T., Sproat, E. A., Lai, Y., Shephard, N. E. and Dillard, D. A., *J. Adhesion* **60**, 153 (1997).
[22] Dillard, D. A., Chen, B., Chang, T. and Lai, Y. -H., *J. Adhesion* **69**, 99 (1999).
[23] Giunta, R. K. and Kander, R. G., *Polym. Eng. & Sci., submitted.*
[24] Parvatareddy, H., *Durability of Polyimide Adhesives and Their Bonded Joints for High Temperature Applications*, Ph.D. Dissertation, Virginia Polytechnic Institute and State University (1997).
[25] XPS International, Inc., http://www.xpsdata.com
[26] Pertsin, A. J. and Pashunin, Y. M., *Appl. Surf. Sci.* **44**, 171 (1990).
[27] Polzonetti, G., Russo, M. V., Iucci, G. and Furlani, A., *Appl. Surf. Sci.* **72**, 227 (1993).
[28] Davies, M. C., Shakesheff, K. M., Shard, A. G., Domb, A., Roberts, C. J., Tendler, S. J. B. and Williams, P. M., *Macromolecules* **29**, 2205 (1996).
[29] Haring, R. A., Nunes, S. L., McGouey, R. P., Galligan, E. A., Volksen, W., Hedrick, J. L. and Labadie, J., *J. Mater. Res.* **10**, 1028 (1995).
[30] Glefond, N. V. and Igumenov, I. K., *Surf. Sci.* **275**, 323 (1992).
[31] Grunert, W., Schlogl, R. and Karge, H. G., *J. Phys. Chem.* **97**, 8638 (1993).